THE JOURNAL OF PHYSICAL CHEMISTRY C

Article

Cite This: J. Phys. Chem. C 2017, 121, 23693-23704

pubs.acs.org/JPCC

Optical Spectroscopy of Dark and Bright Excitons in CdSe Nanocrystals in High Magnetic Fields

A. Granados del Águila,*[,†,‡,∥] G. Pettinari,[†,‡,⊥] E. Groeneveld,[§] C. de Mello Donegá,[§] D. Vanmaekelbergh,[§] J. C. Maan,[†,‡] and P. C. M. Christianen*[,†,‡]

[†]High Field Magnet Laboratory (HFML - EMFL), Radboud University, 6525 ED Nijmegen, The Netherlands

[‡]Institute for Molecules and Materials, Radboud University, Nijmegen 6525 AJ, The Netherlands

[§]Condensed Matter and Interfaces, Debye Institute for Nanomaterials Science, Princetonplein 1, 3584 CC Utrecht, The Netherlands

Supporting Information

ABSTRACT: Low-temperature polarized and time-resolved photoluminescence spectroscopy in high magnetic fields (up to 30 T) has been used to study the spin-polarization, spin-relaxation, and radiative lifetimes of excitons in wurtzite semiconductor (e.g., CdSe) colloidal nanocrystals. The applied magnetic field leads to a significant degree of circular polarization of the exciton photoluminescence, accompanied by a reduction in the photoluminescence decay time. The circular polarization arises from the Zeeman splitting of exciton levels, whereas lifetime reduction results from a polarization-preserving field-induced mixing of exciton levels. We analyze these experimental findings in terms of a simple model that combines both Zeeman effect and exciton-level mixing, as a function of the relative orientation of the nanocrystal *c*-axis and the magnetic field. This model is able to simultaneously describe the degree of circular polarization and lifetime reduction of the exciton photoluminescence, permitting us to quantify the exciton, electron, and hole *g*-factors.

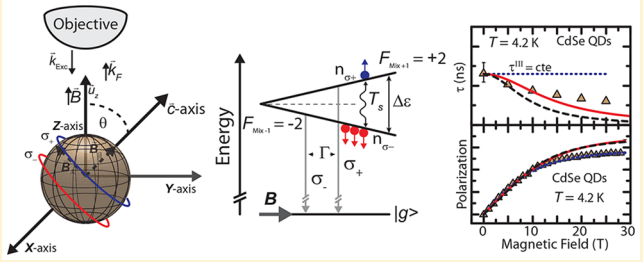

1. INTRODUCTION

Quantum mechanical size confinement of charge carriers in semiconductor nanocrystals (NCs) leads to a discrete, atomic-like, energy level structure. It is well established that the combined effect of an enhanced electron−hole exchange interaction and the internal/shape anisotropy lifts the degeneracy of the bulk exciton manifold, producing a characteristic energy fine-structure of exciton levels. In the common case of wurtzite spherical quantum dots (QDs), such as CdSe QDs, the exciton manifold consists of five distinct states, characterized by their spin projection (F_m) along the nanocrystal *c*-axis. The resulting exciton fine-structure is characterized by a lowest energy exciton state ($F_m = \pm 2$), which is forbidden for direct radiative recombination, thus optically dark, and a higher energy exciton state ($F_m = \pm 1^L$) that is dipole allowed, thus optically bright. The separation between the two levels, denoted by the bright−dark splitting (Δ_{bd}), strongly depends on the QD size because of the size-dependent electron−hole exchange interaction. The exchange splitting Δ_{bd} scales as $\sim 1/R^3$ with R being the QD radius. For typical values of Δ_{bd} of 5−20 meV only the lowest $|F_m| = 2$ level is populated at low temperatures T ($k_BT < \Delta_{bd}$), leading to relatively long exciton lifetimes (~1 μs).[1,2]

Application of a magnetic field ($\vec{B}$) has been shown to be one of the most versatile and powerful tools to investigate the properties of NCs and has been routinely used to unravel the energy fine-structure of excitons in several different systems. An external magnetic field lifts the spin degeneracy of the exciton levels by means of the Zeeman effect. At sufficiently large fields, the Zeeman energy becomes comparable to the exchange interaction, leading to a field-induced mixing of the different exciton levels. The most prominent effect is that the dark $|F_m| = 2$ ground state acquires oscillator strength from the bright $|F_m| = 1$ state, resulting in a significant decrease of the exciton lifetime with increasing field. This effect has been directly observed in a large variety of semiconductor NCs of several compositions by time-resolved photoluminescence (trPL).[3−8] Alternatively, the optical activation of the dark exciton by magnetic fields has been demonstrated by other experimental techniques, such as fluorescence line narrowing (FLN)[9−12] and polarization-resolved photoluminescence (PL).[5,6,11]

A second pronounced effect of the application of a magnetic field is that the Zeeman splitting of the exciton levels leads to a pronounced circular polarization of the nonresonantly excited PL emission. From standard modeling of the field-dependent polarization an effective exciton *g*-factor can be extracted. Remarkably, the actual *g*-values (i.e., Zeeman energies) obtained by this method do not match those determined from theoretical calculations[13−15] and those obtained from

Received: June 23, 2017
Revised: September 1, 2017
Published: September 5, 2017

DOI: 10.1021/acs.jpcc.7b06170
J. Phys. Chem. C 2017, 121, 23693−23704

experiments using FLN[10−12] or single-dot spectroscopy,[16,17] time-resolved Faraday rotation experiments,[18] or magnetic circular dichroism measurements.[13] It should be emphasized that the standard model for the degree of circular polarization does not take into account the field-induced reduction of the exciton lifetime. Nevertheless, exciton *g*-factors determined from circularly polarized emission of ensembles of QDs are frequently used to characterize the magnetic properties of the ensembles.[6,19−23] In this work, we present a detailed analysis of the low-temperature polarization- and time-resolved magneto-PL of ensembles of randomly oriented CdSe QDs as a function of quantum dot size. For all samples we measure the degree of circular polarization (DCP), spin relaxation, and radiative lifetimes of the lowest exciton state as a function of magnetic fields up to 30 T. We analyze the results in terms of three relatively simple two-level bright−dark exciton models, taking into account all relevant magnetic field effects (Zeeman splitting and field-induced exciton mixing). The first (I) and second (II) models determine both the field-dependent DCP and the exciton lifetime in the low- and high-field limit, respectively. The third model (III) is the widely used one for modeling the DCP, where the exciton lifetime does not depend on magnetic field. We find out that models I and II both accurately describe our experimental polarization and lifetime results, leading to values for the exciton *g*-factors that compare reasonably well to those obtained by other direct spectroscopic methods reported in the literature. In contrast, the regularly used DCP model (model III) significantly underestimates the exciton *g*-factor because it does not take properly into account the reduction of the lifetime with magnetic field. In addition, our models I and II also provide reasonable values for the separate electron and hole *g*-factors of our nanocrystals, values that are still relatively scarcely reported in the literature.[24]

This paper is organized as follows: in Section 2 we provide the theoretical background of the magneto-optical properties of spherical wurtzite semiconductor nanocrystals. We introduce the effect of the Zeeman energy and level mixing as a function of magnetic field strength and relative orientation with the nanocrystal *c*-axis. We derive in Section 2.1 a formula that calculates the DCP of the exciton emission as a function of the Zeeman splitting. We introduce, then, in Sections 2.2 and 2.3, three different models depending on the relative importance of the Zeeman energy and the electron−hole exchange energy. For each of the models, we give expressions for the field-dependent energy levels, the *g*-factors, the lifetimes, and the DCP. In Section 3 we present experimental data obtained on several spherical CdSe QDs with different sizes. The experimental results with the predictions of the different theoretical models are compared and extensively discussed in Section 4. The paper is concluded with a summary of the most important findings in Section 5.

2. THEORY

In a colloidal semiconductor QD, the effect of an external magnetic field on the band-edge exciton is given by the Zeeman effect on the separate electrons and holes. Efros et al.[9] first derived the Hamiltonian matrix for wurtzite NCs, allowing for a reasonable description of the exciton energy levels in an applied magnetic field. Equation 30 in ref 9 shows that there are two main effects of the magnetic field on the exciton levels, which depend on the orientation of the field relative to the wurtzite *c*-axis of the NCs (Figure 1). In general, for a QD oriented at an angle θ, the parallel component of the magnetic field

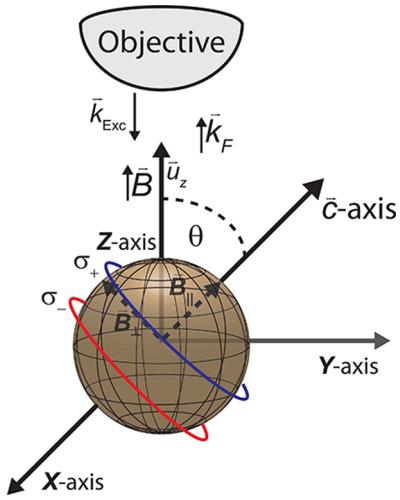

Figure 1. Schematic representation of a spherical wurtzite QD. The nanocrystal *c*-axis makes an angle θ with the applied external magnetic field $\vec{B}$, the observation direction $\vec{u}_z$, and the direction of the laser excitation $\vec{k}_{Exc}$ (Faraday geometry). $\vec{k}_F$ represents the direction of an emitted photon from an exciton state with angular momentum projection F along the *c*-axis.

($B_{\parallel} = B \cos \theta$) leads to a Zeeman splitting of the $F_m = \pm 2$ and $F_m = \pm 1^L$ exciton levels that are doubly degenerate at zero field. The combined effect of the Zeeman splitting, optical selection rules, and level population gives rise to circularly polarized photoluminescence emission. Second, the perpendicular component of the $\vec{B}$-field ($B_{\perp} = B \sin \theta$) mixes the optically forbidden $F_m = +2$ (-2) dark exciton level with the optically allowed $F_m = +1^L$ (-1^L) bright exciton ones, respectively. The admixture between bright and dark wavefunctions allows for *direct* radiative recombination of the optically forbidden exciton states and has, therefore, a direct influence on the exciton lifetime as measured by photoluminescence.

2.1. Zeeman Effect and Degree of Circular Polarization of PL Emission. At sufficiently low temperatures (typically $\sim T \leq 10$ K) and/or in a strong external magnetic field, the PL intensity of an ensemble of randomly oriented QDs gets significantly circularly polarized,[5,6,20,21] as a result of the different exciton populations among the Zeeman sublevels. Analysis of the magnetic field-induced DCP leads, therefore, to information about the Zeeman splitting energy ($\Delta\epsilon$) and the corresponding *g*-factors.

To calculate the magnetic field-induced DCP of the exciton PL emission we introduce a simple two-level model (Figure 2). The ground state exciton level with $F_m = \pm 2$ splits up due to the Zeeman effect, which leads to a (re)distribution of excitons over the Zeeman sublevels. The rate equations of the exciton populations n_{σ_+} ($F_m = +2$) and n_{σ_-} ($F_m = -2$) can be written as

$$\frac{dn_{\sigma_+}}{dt} = G_{\sigma_+} - \frac{n_{\sigma_+}}{\tau_{|F_m|=2}(B, \theta, \eta)} - \frac{n_{\sigma_+}P_{\sigma_+}}{T_s} + \frac{n_{\sigma_-}P_{\sigma_-}}{T_s}, \quad (1a)$$

$$\frac{dn_{\sigma_-}}{dt} = G_{\sigma_-} - \frac{n_{\sigma_-}}{\tau_{|F_m|=2}(B, \theta, \eta)} - \frac{n_{\sigma_-}P_{\sigma_-}}{T_s} + \frac{n_{\sigma_+}P_{\sigma_+}}{T_s}, \quad (1b)$$

where $G_{\sigma_\pm}$ is the generation rate and the $\frac{n_i P_i}{T_s}$ terms account for the spin-relaxation processes between the two Zeeman sublevels, with T_s being the spin relaxation time and $P_i = n_i/\sum_i n_i$ the thermal occupation probability of the level.

DOI: 10.1021/acs.jpcc.7b06170
J. Phys. Chem. C 2017, 121, 23693−23704

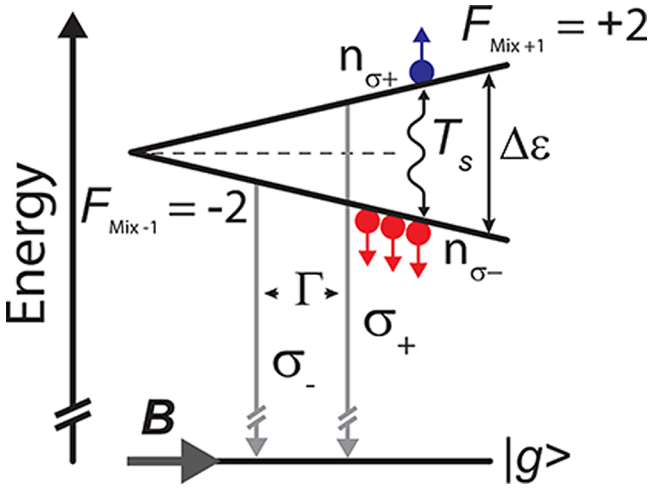

Figure 2. Schematic representation of the exciton levels and symbols used in the models (see text).

When spin relaxation is much faster than recombination, $T_s \ll \tau$, the level occupation follows a Boltzmann distribution ($n_i \propto \exp(\epsilon_i/k_BT)$), with k_B as the Boltzmann constant and T the temperature. The population distribution depends, therefore, on the temperature and the Zeeman splitting energy $\Delta\epsilon = \Delta\epsilon_{|F_m|=2} = \epsilon_{F_m=+2} - \epsilon_{F_m=-2}$, the latter depending not only on the field strength and the angle θ but also on the type of model that is used (see below).

The n_i/τ terms ($i = \sigma_\pm$) are the recombination rates from the two levels, where τ ($\Gamma = \frac{1}{\tau}$) is the exciton lifetime. Since the $F_m = +2$ (-2) state predominantly mixes with the $F_m = +1^L$ (-1^L) state we assume that the $F_m = +2$ (-2) ground exciton states emit σ_+ (σ_-) polarized light, as imposed by the optical selection rules.[5,6] Within the electric dipole approximation, the relative probabilities of detecting $\sigma_\pm$ light components for the $F_m = +1$ exciton in a QD with the c-axis oriented at an angle θ with respect to $\vec{B}$ and $\vec{k}$ (Figure 1) are given by $P_{F_m=+1}(\sigma_\pm) \propto (1 \pm \cos(\theta))^2$. For the oppositely oriented $F_m = -1$ exciton, these probabilities are reversed and given by $P_{F_m=-1}(\sigma_\pm) \propto (1 \mp \cos(\theta))^2$. The detected intensities for $\sigma_\pm$ polarized light emitted from the $F_m = \pm 2$ level with a bright exciton admixture are

$$I_{\sigma_+} = (1 + \cos(\theta))^2 n_{\sigma_+} + (1 - \cos(\theta))^2 n_{\sigma_-}, \tag{2a}$$

$$I_{\sigma_-} = (1 - \cos(\theta))^2 n_{\sigma_+} + (1 + \cos(\theta))^2 n_{\sigma_-}. \tag{2b}$$

A steady-state circularly polarized PL emission corresponds to the situation when a dynamical equilibrium between the two exciton spin populations is reached. The equilibrium population is determined by the competition between the spin relaxation and the radiative recombination rates. For CdSe QDs, it has been observed,[5,6] and will also be shown later in this paper, that the spin-relaxation processes are faster than ~1 ns, which is at least two orders of magnitude faster than the radiative lifetime (~1 μs). Thus, we can safely neglect the ratio $T_s/\tau_{|F|=2}$ and integrate over all orientation angles. The resulting expression for the steady-state DCP, defined as $(I_{\sigma_-} - I_{\sigma_+})/(I_{\sigma_-} + I_{\sigma_+})$, is given by

$$\mathrm{DCP} = \frac{\int_\pi^0 2\tau_{|F_m|=2}\tanh(\Delta\epsilon_{|F|=2}\beta/2)\cos\theta\,\sin\theta\mathrm{d}\theta}{\int_\pi^0 \tau_{|F_m|=2}(1 + \cos^2\theta)\sin\theta\mathrm{d}\theta}, \tag{3}$$

where $\beta = (k_BT)^{-1}$.

2.2. Zeeman Energy versus Exchange Interaction: Different Regimes. The effect of the magnetic field comes on top of the electron–hole exchange and the internal/shape anisotropy, and thus the final magneto-response of a wurtzite QD depends strongly on the ratio between the Zeeman energy $\Delta\epsilon_z$ and the strength of the exchange interaction η. Therefore, it is useful to classify the magnetic field effect on a QD of a given size into different regimes according to the magnitude of η or to the value of the bright–dark splitting, Δ_{bd}, which scales as $\Delta_{bd} \sim 3\eta$.

Regime-I: *Low-field approximation, small nanocrystals.* Small nanocrystals, with R typically below 1.5 nm, have a relatively large exchange energy and a large Δ_{bd} of the order of ~10 meV.[3] In this regime the applied magnetic field can be considered as a perturbation because even at high fields the Zeeman energy is much smaller than the exchange energy. We assign QDs to regime-I when their exchange energy is greater than or comparable to the Zeeman energy of a free electron ($\eta \geq g_e^0\mu_B B$; $g_e^0 = 2$) at 30 T (~3.4 meV). We use a classification based on electrons because the hole g-factor is constant within the framework of the effective mass approximation. Furthermore, tight-binding calculations show that the hole g-factor is very sensitive to crystal anisotropies and shape asymmetries[15] and thus less suitable for our purpose.

Regime-II: *High-field approximation, large nanocrystals.* Large nanocrystals, with R typically above 3 nm, show a small Δ_{bd} of approximately ~1 meV.[3,17] In this case the magnetic field cannot be considered as a perturbation because the Zeeman energy is of the same order of magnitude as the exchange energy. QDs belong to regime-II when their exchange energy is lower than or comparable to the Zeeman energy of a bulk CdSe electron ($\eta \leq g_e^{Bulk}\mu_B B$) at 30 T (~1.2 meV).

2.3. Different Models. In the following we calculate the degree of circular polarization and the decay times of the exciton PL in ensembles of wurtzite QDs using three different models.

2.3.1. Model I: Low-Field Approximation. Treating the magnetic field as a perturbation for small nanocrystals ($g_e^0\mu_B B \leq \eta$), we can make use of eq 30 in ref 9 and of the corresponding exciton wavefunctions given in refs 9 and 25 to obtain the energies of all exciton states in a spherical CdSe nanocrystal and compute the g-factor for each fine-structure exciton level

$$g_{ex,F} = \frac{\epsilon_{F_+} - \epsilon_{F_-}}{\mu_B B}. \tag{4}$$

$\Delta\epsilon_F = \epsilon_{F_+} - \epsilon_{F_-}$ corresponds to the Zeeman splitting of the level with given angular momentum projection F_m. The resulting angle-dependent Zeeman splittings and corresponding g-factors are given by

$$\Delta\epsilon_2 = \epsilon_{+2} - \epsilon_{-2} = g_{ex,2}\mu_B B\cos\theta \ (\text{with } g_{ex,2} = g_e - 3g_h), \tag{5}$$

for the $F_m = \pm 2$ ground–dark state and by

$$\Delta\epsilon_1^L = g_{ex,1^L}\mu_B B\cos\theta \ \ (\text{with } g_{ex,1^L} = (g_e - 3g_h)/2), \tag{6}$$

for the $F_m = \pm 1^L$ bright exciton state.

DOI: 10.1021/acs.jpcc.7b06170
J. Phys. Chem. C 2017, 121, 23693–23704

The average Zeeman splitting for a system of randomly oriented nanocrystals is obtained after integration over all orientation angles in the range $[0, \pi/2]$. Here we treat g_e and g_h as constants, neglecting any anisotropies in the g-factors. We first average over the energy level positions ($\langle \Delta\epsilon_F \rangle = \int_0^{\pi/2} \Delta\epsilon_F \sin\theta$), which leads to $\langle \Delta\epsilon_2 \rangle = g_{ex,2}\mu_B B/2$ for the ground state and $\langle \Delta\epsilon_1^L \rangle = g_{ex,1^L}\mu_B B/2$ for the lowest-energy bright state. Remarkably, both are half of the values given by eqs 5 and 6. A typical result is shown in Figure 3(a) for

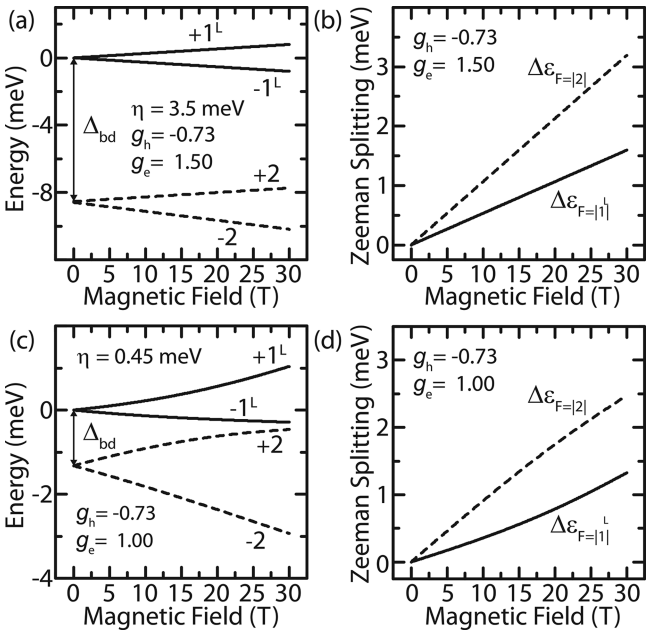

Figure 3. (a) Angular-averaged magnetic field dependence of the lowest-energy bright $|F_m| = 1^L$ and dark $|F_m| = 2$ excitons within model I for an ensemble of wurtzite (R = 1.5 nm) QDs. (b) The resulting Zeeman splitting is shown by dashed ($|F_m| = 2$) and solid ($|F_m| = 1^L$) lines. (c) Same as in (a) but within model II for an ensemble of R = 3 nm wurtzite QDs. (d) The resulting Zeeman splitting for the exciton levels depicted in (c).

a spherical R = 1.5 nm size QD with a calculated exchange energy of η = 3.5 meV ($\Delta_{bd} \sim 9$ meV). The used parameters are $g_h = -0.73$, $g_e = 1.5$, and Δ = 23.75 meV (Δ is the heavy–light hole energy splitting generated by crystal and shape anisotropies). In the figure, the zero-field energy of the bright exciton is taken as reference. Figure 3(b) shows the corresponding ensemble-averaged Zeeman splitting for $F_m = |2|$ (dashed line) and for $F_m = |1^L|$ (solid line), with both splittings increasing linearly with the magnetic field. The splitting of the $F_m = |2|$ exciton is two times larger than that of the bright state, due to its double angular momentum.

In this regime, the quantum-mechanical admixture of the optically active ±1 levels in the dark ±2 exciton state allows for direct optical recombination of the former where the radiative rate of the $F_m = \pm 2$ exciton in an applied magnetic field is given by[9]

$$\frac{1}{\tau^{I}_{|F_m|=2}(B,\theta,\eta)} = \frac{3}{8}\left(\frac{\mu_B B \sin\theta}{\Delta}\right)^2\left(2g_h - g_e\frac{2\eta+\Delta}{3\eta}\right)^2 \frac{1}{\tau_{|F_m|=1^L}}, \quad (7)$$

where $\tau_{|F_m|=1^L}$ is the radiative lifetime of the lowest-energy bright exciton. The lifetime depends on the electron and hole g-factors, field strength B, angle θ, exchange energy (i.e., size) η, and anisotropy Δ.

Briefly, as can be inferred from eqs 5 and 7, magnetic fields parallel to the c-axis ($\theta = 0°$) do not cause bright–dark mixing but have the largest Zeeman splitting. In this orientation, the $F_m = \pm 2$ exciton remains *optically passive*. In contrast, magnetic fields orthogonal to the c-axis ($\theta = 90°$) produce a maximum admixture between dark and bright levels but no Zeeman splitting. As a result, the dark exciton acquires oscillator strength, and its radiative lifetime drastically shortens with increasing the magnetic field. However, in an ensemble experiment and at low temperature (LT), colloidal QDs are randomly orientated and show, although long, a finite lifetime at B = 0 T. To account for this, we introduce a field-independent lifetime τ_o^{LT}[4,7]

$$\frac{1}{\tau^{I}_{|F_m|=2}} = \frac{1}{2\tau^{LT}_{o,|F_m|=2}(\eta)} + \frac{1}{\tau^{I}_{|F_m|=2}(B,\theta,\eta)}. \quad (8)$$

The low-temperature (T = 4.2 K) PL lifetime $\tau^{LT}_{o,|F_m|=2}$ of NCs depends on their size, as is widely reported for CdSe,[1,2] CdTe,[4] ZnSe,[26] and QD heterostructures.[8,27,28] The size dependence originates from the mixing of bright and dark exciton states.[27,28] Specifically, large (small) QDs with a small (large) Δ_{bd} show fast (slow) PL decays. For CdSe and CdTe QDs, this behavior is well reproduced in ref 28 by using a phenomenological expression ($\tau^{LT}_{o,|F_m|=2} \propto \eta$). We used that model to calculate the nominal radiative exciton lifetimes for CdSe QDs lying in the strong (R = 1.5 nm, $\tau^{LT}_{o,|F_m|=2} \sim 600$ ns) and in the weak confinement (R = 3 nm, $\tau^{LT}_{o,|F_m|=2} \sim 100$ ns) regime. The computed values correspond to the zero-field lifetimes in Figure 4(a) and (c), respectively. QD sizes of R = 1.5 nm and R = 3 nm are chosen as representative examples for models I and II, respectively.

For an ensemble of small QDs the angular-average radiative lifetime is obtained by integrating eq 8 over all orientations:

$$\frac{1}{\tau^{I}(B,\eta)} = \frac{1}{\tau^{LT}_{o,|F_m|=2}(\eta)} + \int_0^{\pi} \frac{1}{\tau^{I}_{|F_m|=2}(B,\theta,\eta)} \sin\theta d\theta. \quad (9)$$

The computed model curves with eq 9 are shown in Figure 4(a) for various electron g-factors at a fixed g_h. For this calculation we used $\tau_{|F_m|=1^L}$ = 10 ns and $\tau^{LT}_{o,|F_m|=2}$ = 600 ns, the latter of which corresponds to the low-temperature PL lifetime at B = 0 for a R = 1.5 nm CdSe QD.[1,2,28] The overall trend is that with increasing B the recombination time of the long-lived exciton reduces drastically. With increasing g_e value (curves from top to bottom) the reduction of τ_d^I with B occurs at lower field strengths. In this regime the dark exciton lifetime monotonously decreases with field to saturate only at infinite field strength.

Finally, we discuss the resulting magnetic field-induced circular polarization. Using eqs 3, 5, and 8 (with $\tau^{LT}_{o,|F_m|=2}$ = 600 ns) and the previously used set of parameters η and Δ gives the curves shown in Figure 4(b). The overall behavior is that the DCP increases linearly at low-B-fields and saturates to a value of ~0.8 at high fields. The saturation value at 30 T is well below DCP = 1. The fact that the DCP saturation value is lower than 1 is due to the random orientation of the wurtzite c-axis within the QD ensemble. NCs

DOI: 10.1021/acs.jpcc.7b06170
J. Phys. Chem. C 2017, 121, 23693–23704

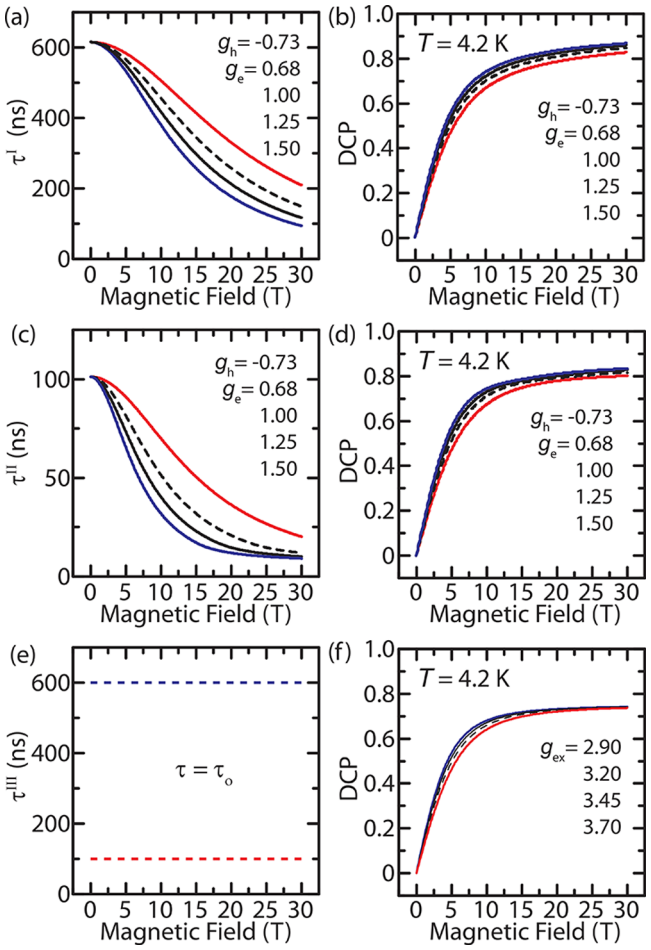

Figure 4. Computed magnetic field dependence for the dark exciton radiative lifetime (a) within model I (eq 9) for an ensemble of wurtzite (R = 1.5 nm) QDs and (b) its degree of circular polarization (eq 3); (c) within model II (eq 16) for R = 3 nm QDs and (d) its degree of circular polarization (eq 3). The modeled curves in (b) and (d) were computed with a fixed hole g_h-factor (g_h = −0.73) and electron g_e-values of g_e = 0.68 (red curves), 1 (black dashed lines), 1.25 (black solid lines), and 1.5 (blue curves). (e) The assumed constant field dependence of the exciton lifetime in model III for R = 1.5 nm (blue dashed line) and R = 3 nm (red dashed line) CdSe QDs. (f) The calculated magnetic field dependence degree of circular polarization of the PL of a randomly oriented bright exciton within model III for g-factors of g_{ex} = 2.9 (red curve), 3.2 (black dashed line), 3.45 (black solid line), and 3.7 (blue solid line).

oriented at larger angles do not exhibit any appreciable Zeeman splitting, and they, therefore, do not contribute to the DCP. Variation of the electron g-factor in the 0.68−1.5 range only marginally affects the exciton g-factor, and therefore, its effect on the DCP is small. Nevertheless, with increasing $g_{ex,2}$ the slope of the linear part increases, and the start of the plateau of the DCP is slightly shifted to higher values. As a result, from the experimental DCP the ground−dark exciton $g_{ex,2}$ value can be deduced. In this model the polarization never fully saturates, which is a direct result of the behavior of the dark exciton recombination time (see Figure 4(a)).

2.3.2. Model II: High-Field Approximation. For large nanocrystals ($\eta \sim g_e^{Bulk}\mu_B B$), the magnetic energy of the lowest exciton states can be exactly obtained.[9] In this regime one finds that the optically dark sublevels $F_m = \pm 2$ are heavily mixed with the bright $F_m = \pm 1^L$ sublevels, leading to the following expressions for the groundstate energy[9,25]

$$\epsilon_{-2} = -\frac{\Delta + 3g_h\mu_B B\cos\theta}{2} - \frac{1}{2}\sqrt{(3\eta + g_e\mu_B B\cos\theta)^2 + (g_e\mu_B B\sin\theta)^2}, \quad (10a)$$

$$\epsilon_{+2} = -\frac{\Delta - 3g_h\mu_B B\cos\theta}{2} - \frac{1}{2}\sqrt{(3\eta - g_e\mu_B B\cos\theta)^2 + (g_e\mu_B B\sin\theta)^2}; \quad (10b)$$

while the $F_m = \pm 1^L$ bright exciton levels are given by

$$\epsilon_{-1^L} = -\frac{\Delta + 3g_h\mu_B B\cos\theta}{2} + \frac{1}{2}\sqrt{(3\eta + g_e\mu_B B\cos\theta)^2 + (g_e\mu_B B\sin\theta)^2}, \quad (11a)$$

$$\epsilon_{+1^L} = -\frac{\Delta - 3g_h\mu_B B\cos\theta}{2} + \frac{1}{2}\sqrt{(3\eta - g_e\mu_B B\cos\theta)^2 + (g_e\mu_B B\sin\theta)^2}. \quad (11b)$$

Figure 3(c) shows the magnetic field dependence of the levels after angular averaging of eqs 10 and 11 for a spherical R = 3 nm size QD with η = 0.45 meV ($\Delta_{bd} \sim$ 1.4 meV), g_h = −0.73, g_e = 1, and Δ = 23.75 meV. Also in this case, the zero-field energy of the bright exciton is taken as reference. At low fields, the levels evolve almost linearly, but at higher fields, a clear nonlinear trend is visible because of the mixing of the F_m = +2 and $F_m = -1^L$ level, which leads to an anticrossing between these levels at high fields. The ensemble-averaged Zeeman splittings $\langle\Delta\epsilon_2\rangle$ of $F_m = |2|$ (dashed line) and $\langle\Delta\epsilon_1^L\rangle$ for $F_m = |1^L|$ (solid line) are shown in Figure 3(d). Both splittings increase linearly up to approximately 10 T, at which field the Zeeman energy approximately equals the exchange energy. At higher fields, the Zeeman splittings exhibit nonlinear behavior, but $\langle\Delta\epsilon_2\rangle$ is always larger than $\langle\Delta\epsilon_1^L\rangle$.

The nonlinear field dependencies of the exciton levels and g-factors in this high-field regime are clearly not present in the low-field approximation of Figures 3(a) and (b). It is remarkable that the results of the low-field limit of model II do not match those of model I. In the low-field limit ($g_e\mu_B B/3\eta \ll 1$) of model II, the Zeeman splittings of the levels are approximately given by

$$\Delta\epsilon_2 = \epsilon_{+2} - \epsilon_{-2} \approx (g_e - 3g_h)\mu_B B\cos\theta, \quad (12a)$$

$$\Delta\epsilon_1^L = \epsilon_{+1^L} - \epsilon_{-1^L} \approx -(g_e + 3g_h)\mu_B B\cos\theta. \quad (12b)$$

Using eq 4, the low field g-factors of the $F_m = |1|^L$ and $F_m = |2|$ are then given by

$$g_{ex,2} \approx (g_e - 3g_h), \quad (13a)$$

$$g_{ex,1^L} \approx -(g_e + 3g_h). \quad (13b)$$

The two regimes thus give the same value for $g_{ex,2} = (g_e - 3g_h)$, but $g_{ex,1^L}$ equals $-(g_e + 3g_h)$ in the high-field approximation and $(g_e - 3g_h)/2$ (eq 6) in the low-field approximation. The bright exciton Zeeman splitting in the high-field regime is lower than that in the low-field regime, which must be attributed to the exchange energy dependence (i.e., size-dependence) of the exciton g-factor.[13]

DOI: 10.1021/acs.jpcc.7b06170
J. Phys. Chem. C 2017, 121, 23693−23704

In the high-field approximation, the field dependence of the radiative decay time for the ground−dark exciton is given by[9]

$$\frac{1}{\tau^{II}_{|F_m|=2}(B,\theta,\eta)} = \frac{3}{4\tau_{|F_m|=1^L}} \frac{\sqrt{1+\zeta^2+2\zeta\cos\theta}-1-\zeta\cos\theta}{\sqrt{1+\zeta^2+2\zeta\cos\theta}}, \quad (14)$$

where $\zeta = g_e\mu_B B/3\eta$ and $\tau_{|F_m|=1^L}$ is the bright exciton lifetime. The degree of bright−dark mixing is proportional to ζ, leading to a B-, θ-, and η (i.e., size) -dependent dark exciton lifetime. As in model I, this expression needs to be modified to account for the experimentally observed zero-field lifetime, resulting in

$$\frac{1}{\tau^{II}_{|F_m|=2}} = \frac{1}{2\tau^{LT}_{o,|F_m|=2}(\eta)} + \frac{1}{\tau^{II}_{|F_m|=2}(B,\theta,\eta)}. \quad (15)$$

Integrating eq 15 over all orientation angles, the exciton recombination decay for an ensemble of large QDs is

$$\frac{1}{\tau^{II}(B,\eta)} = \frac{1}{\tau^{LT}_{o,|F_m|=2}(\eta)} + \int_0^\pi \frac{1}{\tau^{II}_{|F_m|=2}(B,\theta,\eta)}\sin\theta d\theta. \quad (16)$$

The computed model curves are shown in Figure 4(c) for fixed g_h and the previously used set of electron g-factors. Here we used $\tau_{|F_m|=1^L} = 10$ ns and $\tau^{LT}_{o,|F_m|=2} = 100$ ns, which corresponds to typical low-temperature PL lifetime at $B = 0$ T for a $R = 3$ nm CdSe QD.[2,17,28] The overall trend is rather similar to the one in the low-field approximation (Figure 4(a)): the recombination time of the long-lived exciton decreases very rapidly with B. The main difference between the two regimes is that in the high-field approximation the lifetime almost fully saturates in fields below 30 T. Specifically, the saturation is reached at lower fields for higher electron g-factors, when the Zeeman energy becomes larger or comparable to the exchange energy.

The magnetic field-induced DCP for large NCs is given by eq 3. We use the analytical expressions of the dark energy levels given in eq 10 to include the exact Zeeman term for large QDs. We include the recombination time of the $F_m = |2|$ exciton given in eq 15 with $\tau^{LT}_{o,|F_m|=2} = 100$ ns and the previously used set of parameters η and Δ. The calculated curves are shown in Figure 4(d) for the same set of electron and hole g-values as in Figure 4(c), thus for different exciton g-factors. The overall behavior is that the DCP first increases linearly at weak fields (up to ∼10 T) and then levels off at the strongest fields, with a limiting value of DCP → 0.8. In this high-field regime, the polarization is already fully saturated at 30 T. The saturation−polarization plateau is a direct consequence of the almost constant value of the ground-dark state lifetime. The limiting value DCP → 0.8 for the dark exciton is an intrinsic property of randomly oriented ensembles of wurtzite NCs. This is because dots with the c-axis oriented perpendicular to $\vec{B}$ are brightest while having zero Zeeman splitting, thus lowering the ensemble DCP. Finally, the slope of the linear variation of the polarization increases with increasing Zeeman energies. The field range where the DCP is linear is the same for both low- and high-field approximations, and it can be used to extract $g_{ex,2}$.

2.3.3. Model III: Field-Independent Exciton Lifetimes (Standard Model). Here, we compare models I and II with the standard approach. In this model the Zeeman splitting used is that given in model I (eq 5). However, now we assume that the ground-dark state lifetime is field-independent (see Figure 4(e)). Then the expression for the polarization degree is equal to the classical form which is widely used[6,19−23] to model the PL circular polarization of NCs

$$\mathrm{DCP} = \frac{\int_\pi^0 2\cos\theta\tanh(\Delta\epsilon\beta/2)\sin\theta d\theta}{\int_\pi^0 (1+\cos^2\theta)\sin\theta d\theta}. \quad (17)$$

Essentially, this scenario assumes that the circular polarization of the dark exciton is equal to that of the $F_m = |1^L|$ optically active exciton.

Figure 4(f) shows the resulting DCP curves for various exciton $g_{ex,2}$-factors. Comparable to the previous two models, the DCP rises linearly very quickly and reaches saturation at 0.75, independently of the exciton $g_{ex,2}$ used. That plateau, DCP → 0.75, is the maximum polarization that can be reached for the *bright* exciton PL, arising from a randomly oriented ensemble of wurtzite QDs with constant PL decay times. In this case the saturation level is equal for all QD sizes due to the constant lifetime of the bright level in magnetic field. Note that within this model the DCP is only sensitive to the exciton $g_{ex,2}$-factors, without access to the underlying electron and hole g-factors.

3. RESULTS

In this section we present a detailed experimental magneto-optical study of CdSe QDs to investigate the magnetic field dependence of the spin-polarization, spin-relaxation, and radiative lifetimes of dark excitons.

3.1. Experimental Methods. Optical experiments at low temperatures were performed on a set of NC ensemble samples, using polarization-resolved PL and trPL. The NC samples were mounted in a homemade optical probe. Laser light was focused on the sample by a singlet lens (10 mm focal length). The same lens was used to collect the PL emission and direct it to the detection set-up (backscattering geometry). The optical probe was mounted inside a liquid helium bath cryostat (4.2 K) inserted in a 50 mm bore Florida-Bitter electromagnet with a maximum field strength of 31 T. For trPL measurements the excitation was provided by a picosecond pulsed diode-laser operating at 485 nm. The PL signal was detected by an avalanche photodiode connected to a single-photon counter (i.e., time-correlated single-photon counting configuration). For static, spectrally resolved PL measurements the same excitation source was used in continuous wave mode. The PL light was guided through a 300 mm long single grating spectrometer (300 grooves/mm grating) and detected by a liquid nitrogen cooled charge couple device (CCD). Cut-off optical filters were used in excitation and detection, for both PL and trPL experiments.

A set of organically capped CdSe type-I QDs were prepared with radius $R = 1.65$, 1.85, 2.15, and 2.5 nm. These nearly spherical NCs were synthesized by hot injection of organometallic precursors into a coordinating solvent mixture, following methods reported by de Mello Donegá et al.,[29] resulting in a size dispersion of ∼10%. The QDs were dispersed in toluene, and the solutions were dropcasted on GaAs substrates. An extra set of type-I CdSe QD samples with a thin CdS−shell inorganic capping was also used with core size $R = 1.75$ nm and three monolayers of CdS shell. They were fabricated following a standard procedure described in ref 30. All investigated samples were extensively characterized by transmission electron microscopy (TEM) and optical spectros-

DOI: 10.1021/acs.jpcc.7b06170
J. Phys. Chem. C 2017, 121, 23693−23704

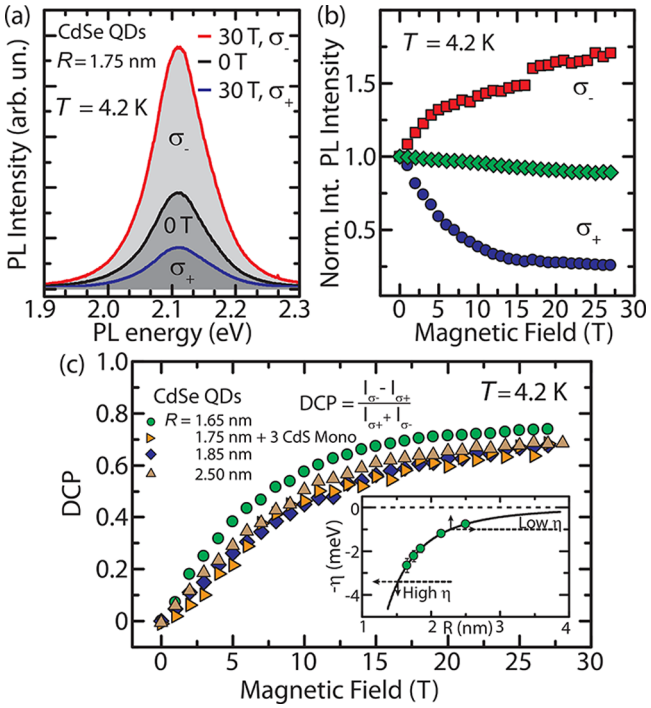

Figure 5. (a) Representative PL ensemble spectra at 0 T (black curve) and 30 T for an R = 1.85 nm CdSe QD at 4.2 K. Red (blue) curves represent the detected σ_- (σ_+) light component intensity. (b) Magnetic field-dependence of the normalized integrated PL intensity for σ_+ (blue circles) and σ_- (red squares) light components. Green diamonds show the unpolarized integrated PL intensity from a frozen solution of the same sample. (c) The experimental low-T steady-state DCP for the various samples. Inset: Calculated size-dependence of the exchange energy given on a negative scale. The exchange energies of the investigated samples are shown by green circles.

copy as reported in refs 2, 29, and 30. Representative TEM images for some of the investigated nearly spherical CdSe NCs are shown as Supporting Information. To further classify the samples we have calculated the theoretical exchange energy of the QDs (symbols in the inset of Figure 5(c)). The values found range from 1 to 3 meV, showing that the QDs used fall within an intermediate magnetic field regime, in between the low- (model I) and high- (model II) field regimes.

3.2. Steady-State Degree of Circular Polarization in High Magnetic Fields. Representative low-temperature PL spectra after nonresonant excitation (laser energy 2.55 eV) for an ensemble of R = 1.75 nm CdSe QDs at 0 T (black curve) and 30 T are shown in Figure 5(a). The PL full-width at half-maximum (fwhm) is ~100 meV and agrees well with the inhomogeneous broadening due to the size dispersion within our QD ensemble samples.[31] At zero field the PL is unpolarized, meaning that the detected amount of σ_+ and σ_- polarized light is equal. In an applied magnetic field, the PL emission gets strongly circularly polarized as seen at 30 T for the σ_- (red curve) and σ_+ (blue curve) PL components.

The magnetic field dependence of the detected integrated intensities for σ_- (I_{σ_-}; red squares) and σ_+ (I_{σ_+}; blue circles) light components is shown in Figure 5(b). I_{σ_-} increases with B at the expense of I_{σ_+}, which decreases. Both intensities saturate at high fields. The total PL intensity is roughly constant with field, as shown by the unpolarized PL intensity of a diluted solution of frozen NCs (green diamonds in Figure 5(b)). We

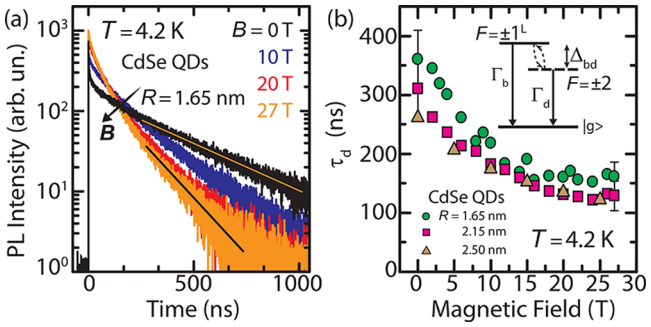

Figure 6. (a) Low-temperature (4.2 K) PL decay curves for an ensemble of randomly oriented R = 1.65 nm CdSe QDs at applied magnetic fields of 0 T (black curve), 10 T (blue curve), 20 T (red curve), and 30 T (orange curve). (b) Magnetic-field evolution of the low-T PL lifetimes of various QD ensemble samples. (Inset) Three-level energy scheme: $|g\rangle$ is the ground state, and F = 1 and F = 2 are the lowest-energy bright and dark levels with radiative recombination decays Γ_b and Γ_d, respectively.

attribute the relatively small drop in intensity (~10%) in the QD solution with increasing magnetic field to an instrumental artifact, i.e., that the focus of the optical set-up varies with field strength. The same holds for the results of the dropcasted sample at B = 17 T, where the intensity suddenly increases (decreases) for σ_- (σ_+) polarized light. Within our experimental accuracy, our data show that the quantum yield (QY) of the QD ensemble is not affected by the magnetic field, in agreement with previous literature.[5] Moreover, it has been shown that high quality organically capped CdSe QDs, as studied here, exhibit near unity QYs at temperatures below ~20 K.[2] As a result, the contribution from nonradiative decay channels to the PL lifetimes can be safely neglected, indicating that the investigated QD single-exponential PL decays are caused by radiative recombination processes.

The degree of circular polarization of the PL at T = 4.2 K is shown in Figure 5(c) for a selection of nanocrystal sizes. Irrespective of the QD radius, $I_{\sigma_-} > I_{\sigma_+}$, leading to a positive sign of the DCP. For all samples the DCP first increases linearly with B (up to 10−15 T) to saturate at high fields at typical values of 0.68−0.73.[5,6] No difference between organically capped CdSe QDs and dots with a CdS shell is observed, confirming that the field-induced circular polarization is an intrinsic property of the core material.

3.3. Dynamic Circular Polarization in High Magnetic Fields: Dark Exciton Recombination and Spin-Relaxation Times. Figure 6(a) shows low-temperature (T = 4.2 K) PL decay curves at selected B-fields for an ensemble of R = 1.65 nm CdSe QDs. The PL decay at zero field shows a biexponential behavior with a fast and a slow decay channel. The fast component is attributed to a transient emission from the higher-energy $|F_m| = 1^L$ bright exciton prior to relaxation to the lowest-energy $|F_m| = 2$ dark exciton state (see inset in Figure 6(b)). The long decay time is related to the radiative recombination lifetime τ_d of the dark exciton level. In field, the long PL decay time dramatically shortens to reach saturation only at the highest fields (~20 T). The magnetic field dependence of the extracted PL decay times is shown in Figure 6(b) for representative QD sizes. The constant τ_d value reached at high fields is typically ~40 to 60% of the zero-field lifetime. Such a strong exciton lifetime reduction is consistent with an F_m = |2| state that becomes optically active through field-induced mixing with the F_m = |1| state.

DOI: 10.1021/acs.jpcc.7b06170
J. Phys. Chem. C 2017, 121, 23693−23704

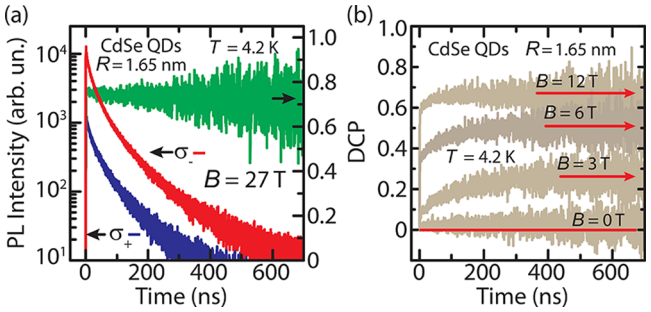

Figure 7. (a) Raw low-temperature time-resolved decay curves for σ_- (red curve) and σ_+ (blue curve) PL components of a randomly oriented R = 1.65 nm CdSe QD ensemble at applied magnetic field of 27 T (left axis). The corresponding DCP is shown by the green curve (right axis). (b) Temporal evolution of the DCP at selected magnetic fields.

Figure 7(a) shows the transient PL traces for the separate σ_- (red curve) and σ_- (blue curve) components at B = 27 T (left axis). Both components display the same, relatively fast, decay time, but the intensity of the σ_- emission is at all times higher than that of the σ_+ emission. The rise of this circular polarization is shown by the green curve in Figure 7(a) (right axis). The dynamic DCP builds up on a subnanosecond time-scale (after photoexcitation at time = 0) to become constant throughout the recombination of dark excitons at longer time delays. The DCP value at the saturation plateau is indicated by arrows in Figure 7. The behavior at low fields is slightly more complex (Figure 7(b)). At fields of a few Tesla the rise of the DCP is relatively slow, but it speeds up with increasing field, until above 12 T the DCP rises almost instantaneously. The exciton spin-relaxation time thus becomes faster with increasing the magnetic field strength until at high fields it is much shorter than the exciton lifetime (T_s < 1 ns). This behavior points to a magnetic field dependent spin-relaxation process, most likely due to field-induced level mixing (see Figure 6), the origin of which needs further theoretical consideration. Importantly, at all magnetic fields the DCP saturates at delay times well within the lifetime of the dark exciton state. Comparing the time-resolved circular polarization values at saturation, indicated by arrows in Figure 7, with the steady-state DCP (see Figure 5(c)), one can see that they are almost identical, suggesting that a finite spin-relaxation time is not a limiting factor for the oberved static PL circular polarization. This result confirms that the observed PL DCP originates from the field-induced changes in the populations of the spin-splitted ground-dark F_m = |2| exciton levels.[5,22,32−34]

4. DISCUSSION

To quantify the g-factors we use a least-squares procedure to fit the experimental DCP and PL decay times within models I, II, and III. For the DCP we use eq 3, and with fitting parameters the electron g_e- and hole g_h-factors in the case of models I and II, whereas for model III the exciton g-factor $g_{ex,2}$ is used. In the case of models I and II, the obtained values for the g-factors are subsequently used to model the PL decay time as a function of magnetic field (eqs 9 and 16), as an additional verification for the fitting accuracy. We note that the decrease of the radiative lifetime at low magnetic fields is mostly sensitive to changes in g_e. For easy comparison of the two models, we show the results of two of the investigated samples with the largest (R = 2.5 nm: Figure 8 (a) and (b)) and smallest (R = 1.65 nm: Figure 8 (c) and (d)) radius, with, respectively, the lowest and highest exchange energies (see inset in Figure 5).

Figure 8(a) shows the fitting curves for the R = 2.5 nm QDs, using model I (red solid line), II (black dashed line), and III (blue dotted line). For the computation, we used η = 0.75 meV (Δ_{bd} ~ 2.23 meV), Δ = 23.75 meV, and τ_o^{LT} = 260 ns. All three curves reproduce nicely the linear variation of the circular polarization, permitting the estimation of the Zeeman energies and effective g-factors. The extracted g_e- and g_h-values are used to reproduce the PL lifetimes in Figure 8(b) by using eq 9 (black dashed line) and eq 16 (red dashed line), with no further fitting parameters. The results are in good agreement with the experiment in the low-field regime, which confirms the validity of our approach and the reliability of the fitted g_e and g_h values. At higher fields the theoretical lifetimes reduce to values below the experimental data. The blue dotted line corresponds to the constant exciton lifetime assumed in model III. The same procedure is used to fit the experimental DCP (green circles in Figure 8(c)) and the PL lifetimes (green circles in Figure 8(d)) for the R = 1.65 nm QDs. For this computation we used η = 2.65 meV (Δ_{bd} ~ 7 meV), Δ = 23.75 meV, and τ_o^{LT} = 360 ns. The same color coding as in Figure 8(a) is used. The three DCP curves are in reasonable agreement with the experiment. The PL lifetime is well reproduced especially at low and intermediate fields.

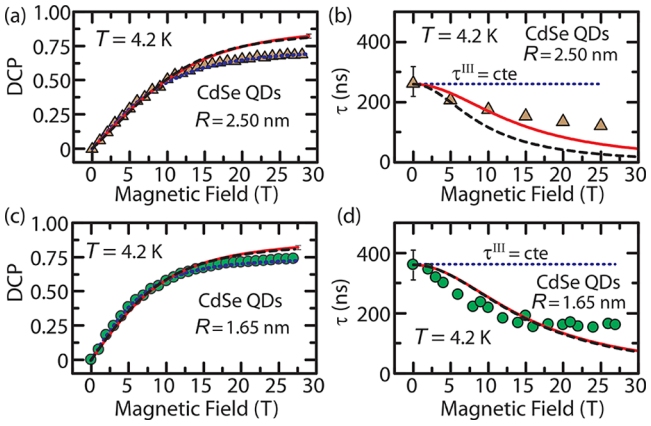

Figure 8. (a) DCP and (b) PL lifetimes of R = 2.5 nm CdSe QDs (brown up-triangles). The lines in (a) are fittings to the data by using model I (red solid line), II (black dashed line), and III (blue dotted line). The lines in (b) are calculated using the obtained electron and hole g-factors (same color code and lines as in (a)). The magnetic field dependent PL lifetime cannot be reproduced by using model III since it is assumed constant, as exemplified by the blue dotted line, clearly highlighting the limitations of model III when applied to dark excitons. (c) DCP and (d) PL lifetimes of R = 1.65 nm QDs (symbols). The lines are obtained using the same procedure as for (a) and (b). Error bars of the fitting procedures for PL lifetimes and DCP are given.

We note that all models are able to qualitatively explain the saturation of the DCP at high fields. Theoretically, this saturation value arises in an ensemble of randomly oriented, wurtzite colloidal quantum dots due to the geometrical averaging of bright exciton emission with field-independent (i.e., constant) decay times (our model III).[9] Our results with models I and II demonstrate that this angle-averaging model also works well when a field-dependent mixing between dark and bright exciton states is specifically taken into account (field-dependent lifetimes). However, models I and II better describe

DOI: 10.1021/acs.jpcc.7b06170
J. Phys. Chem. C 2017, 121, 23693−23704

the actual DCP saturation value for the smaller QDs (Figure 8(c)) than for the larger QDs (Figure 8(a)). Most strikingly, it is clear that the corresponding equations for the lifetimes (eqs 9 and 16) are unable to quantitatively reproduce the high magnetic field behavior found in the experiment (Figure 8(b),(d)). We attribute this observation to the fact that the Efros model[9] assumes that the dark exciton level only couples to the optically allowed, circularly polarized $F_m^{U,L} = |1|$ levels. Within the model, at the highest magnetic fields the $F_m = |2|$ states are fully coupled to the $F_m^{U,L} = |1|$ states, leading to a dark exciton decay as fast as that from the bright levels (~10 ns, see Figure 4), which is in quantitative disagreement with the experimental results. As a matter of fact, the effective-mass approximation used by Efros is unable to explain the PL decay times both at zero magnetic field and in the high field limit. The origin of these discrepancies, which are discussed below, are currently not well understood, and they might be related to each other.

A first possibility is a zero-field mixing of the lowest-energy $F_m = |2|$ state with a higher-energy, noncircularly polarized $F_m = 0^U$ state, which carries a large oscillator strength.[9] This mixing, which might depend on the energy splitting between the states and thus on the electron−hole exchange interaction, as recently suggested experimentally,[27,28] would provide sufficient oscillatory strength for radiative recombination of $F_m = |2|$ excitons. Coupling of the dark exciton state to higher lying bright states has also been theoretically predicted,[35−37] but so far direct experimental evidence is still lacking. Second, transient mixing between bright and dark states mediated by acoustic or optical phonons might increase the probability of $F_m = |2|$ excitons to decay radiatively.[8−12,38−42] Third, the effect of dangling bonds at the QD surface has recently been proposed to alter the recombination process of dark excitons.[43,44] Finally, in the presence of an external magnetic field the spin-forbidden $F_m = |2|$ level additionally couples to $F_m = 1^{U,L}$ states, leading to an extra decrease of its recombination time. In this scenario, in the limit of *high* magnetic fields the dark exciton is fully admixed to all exciton fine-structure states with a lifetime that should become equal to the experimentally observed value of ~150 ns, which is in clear contrast to the predictions of the effective mass model (see Figures 8(b) and (d)).

The values of the electron and holes *g*-factors are shown in Figure 9(a) and (b) as a function of CdSe-QD size, obtained from the DCP fittings when using model I (green squares) and II (blue circles). All error bars are estimated from variations of the electron−hole exchange energy, providing a confident interval for fitting simultaneously the DCP and PL lifetime results. The two scenarios provide similar results for both electrons and holes. The electron values for large NCs are rather similar to that of the bulk CdSe, whereas with decreasing size the electron *g*-factor increases up to $g_e \sim 1.5 \pm 0.10$. These values are in approximate agreement with previous experiments on ensembles,[18] single-dot,[17] and theoretical expectations.[14,15,45] On the other hand, the hole g_h-factor is found to be negative and constant ($g_h \sim -0.17 \pm 0.10$) for all QD dimensions. The obtained hole value is higher than that estimated for bulk CdSe ($g_h \sim -0.73$) and measurements in CdSe NCs.[15,24] For comparison between the fitting methods, the *g*-factors have also been calculated by fitting the PL lifetimes. By using eq 9 (model I) g_e and g_h can be obtained, while using eq 16 (model II) only g_e can be computed. The fitted values are shown in Figure 9(a) and (b) for QD sizes of $R = 1.65$ and 2.5 nm when using models I (green stars) and II (blue diamonds). As seen, they are in approximate agreement with those extracted from the DCP fittings, confirming once more the reliability of our approach. The different values obtained by the different calculation methods provide a confidence interval for the electron and hole *g*-factors. In contrast, the dark exciton $g_{ex,2}$ is constrained to a much more narrow range (see below).

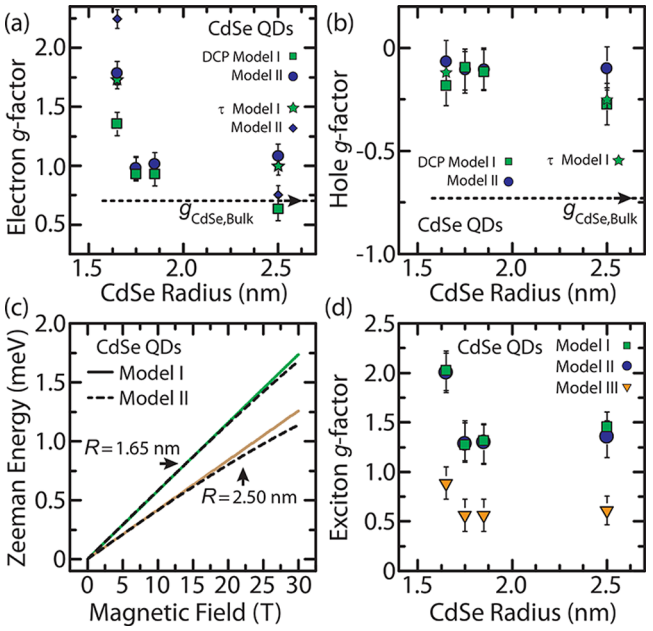

Figure 9. Size-dependence of the electron (a) and hole (b) *g*-factors. The $g_{e,h}$ values are obtained by modeling the steady-state DCP with models I (blue circles) and II (green squares). The dashed lines represent the g_e (0.68) and g_h (−0.73) of bulk CdSe. For comparison, electron and hole *g*-factors computed by fitting the PL lifetimes with models I (green stars) and II (blue diamonds) are given (see text). (c) Calculated (orientation averaged) Zeeman splitting for $R = 1.65$ nm and $R = 2.5$ nm ensemble samples by using values from (a) and (b) with eq 5 (solid lines) and eq 10 (dashed lines). (d) Size-dependence of the exciton *g*-factors. Blue and green symbols are obtained by using electron and hole values from (a) and (b) in the expression $g_{ex,2} = g_e - 3g_h$. Orange down-triangles show the calculated exciton *g*-factors by using the bright exciton scenario (model III).

Using the obtained values of g_e and g_h, the Zeeman energies of the dark exciton levels in the low- and high-field regimes can be computed by using eq 5 and eq 10, respectively. The angular averaged Zeeman splittings for models I (colored solid lines) and II (black dashed lines) are shown in Figure 9(c) as a function of the magnetic field. By definition within model I, the Zeeman term scales linearly with the exciton $g_{ex,2}$-factor given by eq 5. For model II, the magnetic splitting is almost similar to that of model I, experiencing almost the same linear trend. Therefore, for NCs in the high-field regime the exciton $g_{ex,2}$-factor can be extracted by using eq 13. The computed exciton $g_{ex,2}$-factors are shown in Figure 9(d), where blue circles and green squares are obtained from the Zeeman splittings shown in Figure 9(c). The use of any of the two dark exciton models (I and II) provides very similar values of $g_{ex,2}$, as expected from the Zeeman energy analysis. Orange down-triangles represent the calculated values by using model III which are similar to the outcome of previous magneto-PL experiments in CdSe[6] and CdSe/CdS QD[22] ensembles, where the bright exciton model was used.

DOI: 10.1021/acs.jpcc.7b06170
J. Phys. Chem. C 2017, 121, 23693−23704

We focus on the remarkable differences between the results of the dark (models I and II) and the bright exciton (model III) models to describe the polarization. The dark exciton models provide exciton *g*-factors that are in approximate agreement to that extracted for bright and dark excitons from magneto-FLN,[10−12] single-dot experiments,[16,17] and ensemble[13,18] measurements. On the other hand, the regularly used bright exciton model leads to lower exciton *g*-factors, far from direct spectroscopic methods or theoretical estimations.[13,14] Because in model III the exciton recombination time is field-independent (i.e., constant), the Zeeman splitting of the ground-dark exciton is considerably underestimated. Hence, model III can be regarded as suitable to describe the behavior of bright excitons in magnetic fields but is clearly not appropriate to describe the magnetic response of dark excitons when field-induced level mixing is important. Therefore, when modeling the linear variation of the PL circular polarization of nanoscale long-lived excitons, their field-dependent lifetime must be included.

Models I and II reproduce most of the magneto-optical features and provide values of all electron and exciton *g*-factors that compare well to theory and some other experimental methods. However, those models have some limitations as well: (1) The experimental DCP gets a clear saturation plateau at lower values than those predicted by the computations. (2) The monotonic decrease of the theoretically calculated dark exciton recombination times is stronger than the reduction of the experimentally measured PL decay time (see Figure 8(b),(d)). (3) The calculations require a zero-field lifetime τ_o^{LT} to fit simultaneously the PL DCP and the decay times. All these limitations might originate from the simple assumption that $F_m = |2|$ excitons couple only to circularly polarized $F_m = |1|^{U,L}$ bright exciton states, wrongly predicting a monotonic decrease of the dark exciton lifetime. For the CdSe QDs studied here, the saturation of the PL lifetimes occurs at *B*-fields larger than ∼15 T (see Figures 8(b) and (d)). Therefore, in the high-field regime ($B \geq 15$ T) $F_m = |2|$ dark states can be regarded to behave similarly as bright excitons, being the reason why models I and II cannot reproduce entirely the DCP saturation as compared to model III (bright exciton model). This is particularly clear in the polarization curve of the largest size QD samples (see Figure 8(a) and (c)). A complete theory that accounts for all brightening mechanisms of dark excitons, including phonon-assisted transitions,[8−11] mixing of bright and dark levels due to acoustic phonon excitations,[12,38−42] zero-field mixing to noncircularly polarized ($F_m = 0^U$) states,[35−37] dangling bonds,[43,44] unpassivated surface sites,[46] and magnetic-field-induced mixing with circularly polarized ($F_m = |1|^{U,L}$) excitons,[9] is still lacking and might explain some of the limitations of models I and II in the high-field regime.

Long-lived excitons have been reported in a large number of colloidal NCs, with different chemical composition (CdSe, CdTe, InAs, PbSe, and ZnSe) or with distinct morphologies, ranging from nearly spherical to rod-like shapes or in heterostructured NCs.[7,23,26,38,47,48] Despite that the exciton-fine structure is unique for each NC type, in most of the cases light emission at low temperatures is dominated by dark excitons that are energetically close to bright states.[7,26,38,47] Magnetic field-induced brightening of these long-lived excitons have been extensively verified in several NC systems;[7,8,23] therefore, the proposed models I and II might provide an useful scenario to describe the magneto-optical response of NC dark excitons. In particular, models I and II must be valid for similar excitonic fine-structures as discussed here. For instance, they must apply for wurtzite and zinc-blende QDs with asymmetric shapes,[4,9] whose lowest-energy level is the dark $F_m = |2|$ exciton, right below a bright $F_m = |1|$ exciton state. For NCs with large shape anisotropies, such as CdSe quantum rods,[47,49] the discussed models may better be considered qualitatively, due to the different symmetry of the lowest-energy exciton. We hope that our results and analysis will stimulate and support additional theoretical efforts to calculate the magneto-optical response of NCs with different crystal structures and morphologies without the necessity to consider the low- or high-field limit because practical QD sizes are situated in the intermediate regime.

5. CONCLUSION

A strong external magnetic field induces a significant degree of circular polarization, up to 75%, in the emission of a randomly oriented ensemble of wurtzite CdSe QDs. Time-resolved PL decays clearly show a magnetic field-induced, polarization preserving, bright−dark exciton admixture leading to accelerated dark exciton recombination times, where the DCP remains constant throughout the entire $|F_m| = 2$ exciton lifetime. Using rate equations, we have presented a relatively simple model that includes the magnetic field dependence of the ground-dark exciton recombination time that simultaneously reproduces the DCP and PL lifetimes. Fitting the linear variation of the static circular polarization provides quantitative information about the exciton, electron, and hole *g*-factors. The obtained *g*-values are in approximate agreement with those in the current literature. The widely used bright exciton model considerably underestimates the Zeeman term when applied to dark excitons. We have shown that any attempt to model the linear variation of the PL circular polarization of nanoscale long-lived excitons must include the magnetic field dependence on their lifetime.

■ ASSOCIATED CONTENT

Supporting Information

The Supporting Information is available free of charge on the ACS Publications website at DOI: 10.1021/acs.jpcc.7b06170.

Supporting figures and supporting methods (PDF)

■ AUTHOR INFORMATION

Corresponding Authors

*E-mail: a.granadosdelaguila@ntu.edu.sg.
*E-mail: p.christianen@science.ru.nl.

ORCID

A. Granados del Águila: 0000-0002-8162-7192
C. de Mello Donegá: 0000-0002-4403-3627
D. Vanmaekelbergh: 0000-0002-3535-8366

Present Addresses

[‖]Division of Physics and Applied Physics, School of Physical and Mathematical Sciences, Nanyang Technological University, Singpore 637371, Singapore.
[⊥]National Research Council, Institute for Photonics and Nanotechnologies (IFN-CNR), Via Cineto Romano 42, 00156 Rome, Italy.

Notes

The authors declare no competing financial interest.

DOI: 10.1021/acs.jpcc.7b06170
J. Phys. Chem. C 2017, 121, 23693−23704

■ ACKNOWLEDGMENTS

We acknowledge the support of HFML-RU/FOM, member of the European Magnetic Field Laboratory (EMFL). Part of this work has been supported by EuroMagNET II under the EU contract number 228043.

■ REFERENCES

(1) Crooker, S. A.; Barrick, T.; Hollingsworth, J. A.; Klimov, V. I. Multiple Temperature Regimes of Radiative Decay in CdSe Nanocrystal Quantum Dots: Intrinsic Limits to the Dark-Exciton Lifetime. *Appl. Phys. Lett.* **2003**, *82*, 2793−2795.

(2) de Mello Donegá, C.; Bode, M.; Meijerink, A. Size- and Temperature-Dependence of Exciton Lifetimes in CdSe Quantum Dots. *Phys. Rev. B* **2006**, *74*, 085320.

(3) Nirmal, M.; Norris, D. J.; Kuno, M.; Bawendi, M. G.; Efros, A. L.; Rosen, M. Observation of the "Dark Exciton" in CdSe Quantum Dots. *Phys. Rev. Lett.* **1995**, *75*, 3728−3731.

(4) Blokland, J. H.; Claessen, V. I.; Wijnen, F. J. P.; Groeneveld, E.; de Mello Donegá, C.; Vanmaekelbergh, D.; Meijerink, A.; Maan, J. C.; Christianen, P. C. M. Exciton Lifetimes of CdTe Nanocrystal Quantum Dots in High Magnetic Fields. *Phys. Rev. B* **2011**, *83*, 035304.

(5) Furis, M.; Hollingsworth, J. A.; Klimov, V. I.; Crooker, S. A. Time- and Polarization-Resolved Optical Spectroscopy of Colloidal CdSe Nanocrystal Quantum Dots in High Magnetic Fields. *J. Phys. Chem. B* **2005**, *109*, 15332−15338.

(6) Johnston-Halperin, E.; Awschalom, D. D.; Crooker, S. A.; Efros, A. L.; Rosen, M.; Peng, X.; Alivisatos, A. P. Spin Spectroscopy of Dark Excitons in CdSe Quantum Dots to 60 T. *Phys. Rev. B* **2001**, *63*, 205309.

(7) Schaller, R. D.; Crooker, S. A.; Bussian, D. A.; Pietryga, J. M.; Joo, J.; Klimov, V. I. Revealing the Exciton Fine Structure of PbSe Nanocrystal Quantum Dots Using Optical Spectroscopy in High Magnetic Fields. *Phys. Rev. Lett.* **2010**, *105*, 067403.

(8) Brovelli, S.; Schaller, R. D.; Crooker, S. A.; García-Santamaría, F.; Chen, Y.; Viswanatha, R.; Hollingsworth, J. A.; Htoon, H.; Klimov, V. I. Nano-Engineered Electron-Hole Exchange Interaction Controls Exciton Dynamics in Core-Shell Semiconductor Nanocrystals. *Nat. Commun.* **2011**, *2*, 280.

(9) Efros, A. L.; Rosen, M.; Kuno, M.; Nirmal, M.; Norris, D. J.; Bawendi, M. Band-Edge Exciton in Quantum Dots of Semiconductors with a Degenerate Valence Band: Dark and Bright Exciton States. *Phys. Rev. B* **1996**, *54*, 4843−4856.

(10) Furis, M.; Htoon, H.; Petruska, M. A.; Klimov, V. I.; Barrick, T.; Crooker, S. A. Bright-Exciton Fine Structure and Anisotropic Exchange in CdSe Nanocrystal Quantum Dots. *Phys. Rev. B* **2006**, *73*, 241313.

(11) Wijnen, F. J. P.; Blokland, J. H.; Chin, P. T. K.; Christianen, P. C. M.; Maan, J. C. Competition between Zero-Phonon and Phonon-Assisted Luminescence in Colloidal CdSe Quantum Dots. *Phys. Rev. B* **2008**, *78*, 235318.

(12) Granados del Águila, A.; Jha, B.; Pietra, F.; Groeneveld, E.; de Mello Donegá, C.; Maan, J. C.; Vanmaekelbergh, D.; Christianen, P. C. M. Observation of the Full Exciton and Phonon Fine Structure in CdSe/CdS Dot-in-Rod Heteronanocrystals. *ACS Nano* **2014**, *8*, 5921−5931.

(13) Kuno, M.; Nirmal, M.; Bawendi, M. G.; Efros, A.; Rosen, M. Magnetic Circular Dichroism Study of CdSe Quantum Dots. *J. Chem. Phys.* **1998**, *108*, 4242−4247.

(14) Schrier, J.; Birgitta Whaley, K. Tight-binding *g*-factor Calculations of CdSe Nanostructures. *Phys. Rev. B* **2003**, *67*, 235301.

(15) Chen, P.; Whaley, K. Magneto-Optical Response of CdSe Nanostructures. *Phys. Rev. B* **2004**, *70*, 045311.

(16) Htoon, H.; Crooker, S. A.; Furis, M.; Jeong, S.; Efros, A. L.; Klimov, V. I. Anomalous Circular Polarization of Photoluminescence Spectra of Individual CdSe Nanocrystals in an Applied Magnetic Field. *Phys. Rev. Lett.* **2009**, *102*, 017402.

(17) Biadala, L.; Louyer, Y.; Tamarat, P.; Lounis, B. Band-Edge Exciton Fine Structure of Single CdSe/ZnS Nanocrystals in External Magnetic Fields. *Phys. Rev. Lett.* **2010**, *105*, 157402.

(18) Gupta, J. A.; Awschalom, D. D.; Efros, A. L.; Rodina, A. V. Spin Dynamics in Semiconductor Nanocrystals. *Phys. Rev. B* **2002**, *66*, 125307.

(19) Chamarro, M.; Gourdon, C.; Lavallard, P. Photoluminescence Polarization of Semiconductor Nanocrystals. *J. Lumin.* **1996**, *70*, 222−237.

(20) Langof, L.; Fradkin, L.; Ehrenfreund, E.; Lifshitz, E.; Micic, O.; Nozik, A. Colloidal InP/ZnS Core-Shell Nanocrystals Studied by Linearly and Circularly Polarized Photoluminescence. *Chem. Phys.* **2004**, *297*, 93−98.

(21) Turyanska, L.; Blokland, J. H.; Elfurawi, U.; Makarovsky, O.; Christianen, P. C. M.; Patanè, A. Photoluminescence of PbS Nanocrystals at High Magnetic Fields up to 30 T. *Phys. Rev. B* **2010**, *82*, 193302.

(22) Liu, F.; Biadala, L.; Rodina, A. V.; Yakovlev, D. R.; Dunker, D.; Javaux, C.; Hermier, J.-P.; Efros, A. L.; Dubertret, B.; Bayer, M. Spin Dynamics of Negatively Charged Excitons in CdSe/CdS Colloidal Nanocrystals. *Phys. Rev. B* **2013**, *88*, 035302.

(23) Liu, F.; Rodina, A. V.; Yakovlev, D. R.; Greilich, A.; Golovatenko, A. A.; Susha, A. S.; Rogach, A. L.; Kusrayev, Y. G.; Bayer, M. Exciton Spin Dynamics of Colloidal CdTe Nanocrystals in Magnetic Fields. *Phys. Rev. B* **2014**, *89*, 115306.

(24) Fernée, M. J.; Sinito, C.; Louyer, Y.; Christian, P.; Tich-Lam, N.; Mulvaney, P.; Tamarat, P.; Brahim, L. Magneto-Optical Properties of Trions in Non-Blinking Charged Nanocrystals Reveal an Acoustic Phonon Bottleneck. *Nat. Commun.* **2012**, *3*, 1287.

(25) Klimov, V. I. *Nanocrystal Quantum Dots*, 2nd ed.; CRC Press, 2010.

(26) Eilers, J.; van Hest, J.; Meijerink, A.; Donega, C. d. M. Unravelling the Size and Temperature Dependence of Exciton Lifetimes in Colloidal ZnSe Quantum Dots. *J. Phys. Chem. C* **2014**, *118*, 23313−23319.

(27) Biadala, L.; Siebers, B.; Gomes, R.; Hens, Z.; Yakovlev, D. R.; Bayer, M. Tuning Energy Splitting and Recombination Dynamics of Dark and Bright Excitons in CdSe/CdS Dot-in-Rod Colloidal Nanostructures. *J. Phys. Chem. C* **2014**, *118*, 22309−22316.

(28) Granados del Águila, A.; Groeneveld, E.; Maan, J. C.; de Mello Donegá, C.; Christianen, P. C. M. Effect of Electron-Hole Overlap and Exchange Interaction on Exciton Radiative Lifetimes of CdTe/CdSe Heteronanocrystals. *ACS Nano* **2016**, *10*, 4102−4110.

(29) de Mello Donegá, C.; Hickey, S. G.; Wuister, S. F.; Vanmaekelbergh, D.; Meijerink, A. Single-Step Synthesis to Control the Photoluminescence Quantum Yield and Size Dispersion of CdSe Nanocrystals. *J. Phys. Chem. B* **2003**, *107*, 489−496.

(30) Chin, P.; Hikmet, R.; Meskers, S.; Janssen, R. Energy Transfer and Polarized Emission in Cadmium Selenide Nanocrystal Solids with Mixed Dimensionality. *Adv. Funct. Mater.* **2007**, *17*, 3829−3835.

(31) Talapin, D. V.; Lee, J.-S.; Kovalenko, M. V.; Shevchenko, E. V. Prospects of Colloidal Nanocrystals for Electronic and Optoelectronic Applications. *Chem. Rev.* **2010**, *110*, 389−458.

(32) Kroutvar, M.; Ducommun, Y.; Heiss, D.; Bichler, M.; Schuh, D.; Abstreiter, G.; Finley, J. J. Optically Programmable Electron Spin Memory using Semiconductor Quantum Dots. *Nature* **2004**, *432*, 81.

(33) Tsitsishvili, E.; Baltz, R. v.; Kalt, H. Exciton Spin Relaxation in Single Semiconductor Quantum Dots. *Phys. Rev. B* **2003**, *67*, 205330.

(34) Oka, Y.; Permogorov, S.; Pittini, R.; Shen, J.; Kayanuma, K.; Reznitsky, A.; Tenishev, L.; Verbin, S. Spin Relaxation Times of Exciton States in ZnCdSe/ZnSe Low Dimensional Heterostructures. *Phys. E* **2001**, *10*, 315−319.

(35) Goupalov, S. V. Anisotropy-Induced Exchange Splitting of Exciton Radiative Doublet in CdSe Nanocrystals. *Phys. Rev. B* **2006**, *74*, 113305.

(36) Califano, M.; Franceschetti, A.; Zunger, A. Lifetime and Polarization of the Radiative Decay of Excitons, Biexcitons, and Trions in CdSe Nanocrystal Quantum Dots. *Phys. Rev. B* **2007**, *75*, 115401.

DOI: 10.1021/acs.jpcc.7b06170
J. Phys. Chem. C 2017, 121, 23693−23704

(37) Rodina, A. V.; Efros, A. L. Radiative Recombination from Dark Excitons in Nanocrystals: Activation Mechanisms and Polarization Properties. *Phys. Rev. B* **2016**, *93*, 155427.
(38) Oron, D.; Aharoni, A.; de Mello Donegá, C.; van Rijssel, J.; Meijerink, A.; Banin, U. Universal Role of Discrete Acoustic Phonons in the Low-Temperature Optical Emission of Colloidal Quantum Dots. *Phys. Rev. Lett.* **2009**, *102*, 177402.
(39) Biadala, L.; Louyer, Y.; Tamarat, P.; Lounis, B. Direct Observation of the Two Lowest Exciton Zero-Phonon Lines in Single CdSe/ZnS Nanocrystals. *Phys. Rev. Lett.* **2009**, *103*, 037404.
(40) Huxter, V. M.; Scholes, G. D. Acoustic Phonon Strain Induced Mixing of the Fine Structure Levels in Colloidal CdSe Quantum Dots Observed by a Polarization Grating Technique. *J. Chem. Phys.* **2010**, *132*, 104506.
(41) Hannah, D. C.; Dunn, N. J.; Ithurria, S.; Talapin, D. V.; Chen, L. X.; Pelton, M.; Schatz, G. C.; Schaller, R. D. Observation of Size-Dependent Thermalization in CdSe Nanocrystals Using Time-Resolved Photoluminescence Spectroscopy. *Phys. Rev. Lett.* **2011**, *107*, 177403.
(42) Werschler, F.; Hinz, C.; Froning, F.; Gumbsheimer, P.; Haase, J.; Negele, C.; de Roo, T.; Mecking, S.; Leitenstorfer, A.; Seletskiy, D. V. Coupling of Excitons and Discrete Acoustic Phonons in Vibrationally Isolated Quantum Emitters. *Nano Lett.* **2016**, *16*, 5861−5865.
(43) Rodina, A.; Efros, A. L. Magnetic Properties of Nonmagnetic Nanostructures: Dangling Bond Magnetic Polaron in CdSe Nanocrystals. *Nano Lett.* **2015**, *15*, 4214−4222.
(44) Biadala, L.; Shornikova, E. V.; Rodina, A. V.; Yakovlev, D. R.; Siebers, B.; Aubert, T.; Nasilowski, M.; Hens, Z.; Dubertret, B.; Efros, A. L. Magnetic Polaron on Dangling-Bond Spins in CdSe Colloidal Nanocrystals. *Nat. Nanotechnol.* **2017**, *12*, 569.
(45) Rodina, A. V.; Efros, A. L.; Alekseev, A. Y. Effect of the Surface on the Electron Quantum Size Levels and Electron g-factor in Spherical Semiconductor Nanocrystals. *Phys. Rev. B* **2003**, *67*, 155312.
(46) Califano, M.; Franceschetti, A.; Zunger, A. Temperature Dependence of Excitonic Radiative Decay in CdSe Quantum Dots: The Role of Surface Hole Traps. *Nano Lett.* **2005**, *5*, 2360−2364.
(47) Le Thomas, N.; Herz, E.; Schöps, O.; Woggon, U.; Artemyev, M. V. Exciton Fine Structure in Single CdSe Nanorods. *Phys. Rev. Lett.* **2005**, *94*, 016803.
(48) Rainò, G.; Stöferle, T.; Moreels, I.; Gomes, R.; Kamal, J. S.; Hens, Z.; Mahrt, R. F. Probing the Wave Function Delocalization in CdSe/CdS Dot-in-Rod Nanocrystals by Time- and Temperature-Resolved Spectroscopy. *ACS Nano* **2011**, *5*, 4031−4036.
(49) Shabaev, A.; Efros, A. L. 1D Exciton Spectroscopy of Semiconductor Nanorods. *Nano Lett.* **2004**, *4*, 1821−1825.

DOI: 10.1021/acs.jpcc.7b06170
J. Phys. Chem. C 2017, 121, 23693−23704